Journal of Catalysis **195,** 1–11 (2000)
doi:10.1006/jcat.2000.2978, available online at http://www.idealibrary.com on IDEAL®

Catalytic Behavior of Supported KNiCa Catalyst and Mechanistic Consideration for Carbon Dioxide Reforming of Methane

Jong-San Chang, Sang-Eon Park,[1] Jung Whan Yoo, and Jin-Nam Park

Catalysis Center for Molecular Engineering, Korea Research Institute of Chemical Technology (KRICT), P.O. Box 107, Yusung, Taejon 305-606, Korea

Received September 17, 1999; revised June 23, 2000; accepted June 23, 2000

Carbon dioxide reforming of methane to synthesis gas has been investigated using a KNiCa catalyst loaded on a highly siliceous NaZSM-5 zeolite support which was promoted with alumina. The catalytic behavior of the supported KNiCa catalyst has also been compared to that of the supported Ni catalyst. Long-time catalytic measurements at 800°C show that the supported KNiCa catalyst has excellent catalyst stability for 140 h due to the promotional effect of surface carbonate species leading to surface enrichment of carbon dioxide, while the supported Ni catalyst is subjected to severe catalyst deactivation due to extensive coke deposition less than 40 h on stream. Pulse reaction, thermogravimetric analysis, isotope experiment, and X-ray absorption spectroscopy have been performed for understanding the detailed chemistry and the mechanistic aspects of the CO_2 reforming. Pulse reaction and thermogravimetric analysis on the supported KNiCa catalyst indicate that methane is activated on the surface Ni species and carbon dioxide interacts with alkaline promoters to form surface carbonates which hinder the formation of inactive coke or scavenge carbon from the surface Ni species. A study of deuterium isotope effects for the reforming reaction shows that there is almost no isotope effect on the supported KNiCa catalyst, suggesting that a CH_4 dissociation step is not rate determining. In this work, mechanistic investgations reveal that reaction between the adsorbed carbon species and the dissociated oxygen atoms on Ni sites of catalyst surface leads to the production of carbon monoxide and the regeneration of metallic nickel species as a consequence, which is assumed to be a rate-determining step in the CO_2 reforming. It is also proposed that the oxidation step of surface carbon with surface oxygen or adsorbed CO_2 as surface carbonate species on the catalyst is important for maintaining catalyst stability of the supported KNiCa by the efficient removal of surface carbon species.

Key Words: **CO_2 reforming of methane; nickel catalyst; zeolite support; catalytic behavior; mechanistic investigation.**

INTRODUCTION

In recent years, carbon dioxide reforming of methane (so-called "dry reforming") to produce synthesis gas is becoming an attractive and challenging subject for the chemical utilization of natural gas and carbon dioxide, which are substances intimately related to the greenhouse effect and energy resources (1). From an industrial viewpoint, the reaction is also potentially beneficial because it produces CO-rich synthesis gas (H_2/CO), in comparison with that from either steam reforming or partial oxidation of methane (2). However, the coke formation over catalysts during the reforming of methane has been regarded as a main reason for catalyst deactivation (3). In particular, coke formation in dry reforming was known to be more serious than for any other reforming reactions (3).

The dry reforming reaction has been studied over numerous supported metal catalysts such as Ni-based catalysts (4–10) as well as supported noble metal catalysts (1, 11–15), which have been found to exhibit promising catalytic performance in terms of methane conversion and selectivity to synthesis gas. The catalysts based on noble metals have been reported to be more active and less sensitive to coking than the Ni-based catalysts (13, 14). However, considering the aspects of high cost and limited availability of noble metals, it is more practical to develop Ni-based catalysts which are resistant to carbon deposition and exhibit high activity for the reaction (8).

To develop a high-performance catalyst, it is essential to elucidate the reaction mechanism (16). In particular, the exact nature of the reaction intermediates arising from the possible sources of carbon and oxygen and their fate in reaction pathways remain open fundamental questions (17). Some mechanistic approaches for supported Ni catalysts have recently been published (16–25). However, the mechanism for this reforming reaction has not been clarified yet. Concerning a rate-determining step of this reaction, there are five different suggestions. Martin *et al.* (18) proposed that dissociation of carbon dioxide over Ni/SiO_2 catalysts is a rate-determining step in dry reforming. Gamman *et al.* (19) claimed that the dissociative chemisorption of CO_2 over Ni/SiO_2 catalysts into its atomic constituents is crucial and the reaction mechanism is associated with dissociatively adsorbed CO_2 and methyl radicals. Methane dissociation was also assumed to be the rate-determining

[1] To whom correspondence should be addressed. Fax: +82-42-860-7676. E-mail: separk@pado.krict.re.kr.

0021-9517/00 $35.00

step in the kinetic studies by Zhang and Verykios (20) and Mirodatos *et al.* (21). They reported that methane activation over Ni/La_2O_3 catalysts is a slow step. In addition, Wang and Au recently found that CH_4 conversion in the dry reforming is higher than CD_4 conversion in the reaction over Ni/SiO_2 catalysts, indicating that methane dissociation would be the rate-determining step (16). They also suggested that based on the observed CH_4/CD_4 isotope effects, there are two different pathways for the formation of CO. Besides the dissociation of methane and carbon dioxide, the reaction between surface carbon or hydrocarbon species and surface oxygen on metallic nickel sites is also considered to be the rate-determining step. Bradford and Vannice, in contrast, suggested two rate-determining steps: methane activation and CH_xO decomposition (22). In their report, adsorbed hydrogen reacts with CO_2 to form CO and an OH group is retained on the support. The OH groups were thought to react at the metal-support interface with CH_x, resulting from methane decomposition, to form CH_xO species which subsequently decompose to CO and H_2. In general, trends in a microkinetic model by Aparicio's report (23) were in agreement with the kinetic model for the dry reforming proposed by Bradford and Vannice (22). In view of the equal rate constant observed between CO and H_2 production, Osaki *et al.* (24) insisted that $CH_x(s) + O(s) \rightarrow CO(s) + xH(s)$ is the rate-determing step. This assumption was proved by pulse surface reaction rate analysis (PSRA) (24) and the kinetic isotope effect by *ab initio* molecular orbital calculation (25). According to Hu and Ruckenstein (26), transient response analysis on Ni/SiO_2 catalysts indicated that the surface reaction between carbon and oxygen species on metallic nickel sites constitutes the rate-determining step of the dry reforming reaction. Miradotos *et al.* (17) proposed that the oxidation step which does not involve any C–H bond activation, i.e., the reaction of surface carbon monomers with surface oxygen atoms into CO, is assumed to be rate limiting since no kinetic isotopic effect is found for the formation of CO under the stoichiometric reforming conditions. However, Rostrup-Nielsen and co-workers (15) reported that replacing steam by CO_2 has no significant impact on the reforming mechanism. When carbon dioxide is added to the feed ($CH_4 + H_2O$), the decreasing rate could in principle be explained by the CO_2 activation becoming the rate-determining step, but this appears unlikely because all catalysts had high rates for reverse water-gas shift (RWGS) reactions. It was more likely that the rates were influenced by the adsorption of carbon monoxide, which has a high concentration under dry reforming conditions. In parallel with this, Baerns and co-workers found that a synergistic interaction between active metal and support was derived for the RWGS reaction which was explained by an additional driving force of the CO_2 dissociation (27).

In addition, the effect of structure sensitivity for the dry reforming should be considered for catalyst design because basic reaction steps such as methane decomposition and CO_2 dissociation are structure sensitive (28, 29). Therefore, taking the previous reports into consideration, it seems likely that the rate-determining step in the dry reforming is greatly dependent on the working catalyst and reaction condition.

We have previously reported that zeolite-supported KNiCa catalysts exhibit high activity as well as strong coke resistance for the dry reforming into synthesis gas (30). The support used for KNiCa catalyst was a highly siliceous NaZSM-5 zeolite mixed with alumina as a binder of zeolite pellet. It was found that this support offered high catalyst stability for the KNiCa catalyst, as compared with γ-Al_2O_3 and SiO_2 supports (32). In addition to elucidation of the reaction mechanism, studies of carbon formation and removal on reforming catalysts are also important for devising more effective and stable catalysts. To understand the detailed chemistry of dry reforming, we investigated the behavior of CO_2 and CH_4 during the reaction, as well as on the catalyst surface. The present work also addresses the mechanistic aspects of the dry reforming reaction using pulse reaction, isotope experimentation, and X-ray absorption spectroscopy.

EXPERIMENTAL

Catalyst Preparation and Testing

Zeolite-supported Ni and KNiCa catalysts were prepared by the molten-salt method and are designated as Ni/ZSI and KNiCa/ZSI, respectively, hereinafter. Detailed procedures of preparation of these catalysts have been described elsewhere (30). The support was a highly siliceous ZSM-5 zeolite (UOP S-115, $S_{BET} = 340$ m^2/g, $Si/Al > 200$) mixed with alumina (19.5 wt%) as a binder for the zeolite pellet. The loading of metallic nickel on both catalysts was 5.3 wt%. The molar ratio of KNiCa oxide in KNiCa/ZSI was $K : Ni : Ca = 0.08 : 1.0 : 2.2$. The total metallic oxide content was 17.9 wt%.

Catalytic measurements for long-time durability tests at 800°C were carried out in a fixed-bed quartz reactor with inner diameter of 4 mm at atmospheric pressure. Before each catalytic measurement, the catalyst measurement, the catalyst was reduced *in situ* at 700°C for 1 h in a 5% H_2/N_2 flow (50 ml/min). The reactant gas stream consisted of carbon dioxide and methane was diluted with nitrogen (molar ratio of $CH_4 : CO_2 : N_2 = 1 : 1 : 2.2$). The flow rate of the feed was $GHSV = 6.0 \times 10^4$ ml/h · g cat. The gas compositions of reactants, products, and nitrogen as an internal standard were analyzed by an on-line gas chromatograph (Chrompack Model CP 9001) equipped with a packed column (Carbosphere) and a thermal conductivity detector.

Gravimetric Analysis

Gravimetric changes of the reduced catalysts during treatment with methane at 600°C were measured by IGA (Intelligent gravimetric analyzer, Hiden IGA-002). Fresh catalyst (ca. 51 mg) was loaded on a sample pan which was placed in a gravimetric chamber for thermogravimetric analysis. Temperature-programmed treatment with CO_2 (CO_2–TPO) on the catalysts pretreated with methane at 600°C and temperature-programmed desorption of CO_2 (CO_2–TPD) of reduced Ni catalysts were also investigated by IGA, coupled with a mass spectrometer (Hiden DSMS).

Pulse Reactions

The gases used—methane (purity: 99.995%), carbon dioxide (99.999%), nitrogen (99.999%), argon (99.999%), and helium (99.999%)—were supplied by Air Products and Korea Standard Gas Co. Experiments using pulse reaction of reactant gases were conducted with a gas sampling valve in a pulse reactor (1/4-inch outer diameter, quartz), which was incorporated between the sample inlet and the column of the gas chromatograph. All the catalysts were reduced in the reactor with 5% H_2/N_2 (50 ml/min) at 700°C for 3 h before use. During the pulse experiments, the flow rate of helium gas through the reactor was kept constant with 30 ml/min and the reactant gas mixture was injected to the reactor by helium carrier gas. Thus the reactant gas was diluted before passing through the reactor. For each measurement, 100 mg of catalyst was used, and one pulse with the sampling loop contained 30.4 μmol of reactant gases.

Deterium Isotope Experiments

Steady-state experiments for determining kinetic isotope effects were performed at 600–700°C and atmospheric pressure by feeding the fixed-bed reactor with the mixtures $CH_4/CO_2/N_2$ or $CD_4/CO_2/N_2$ (24/24/52). Ten miligrams of catalyst was employed in each experiment. The CD_4 had a purity of 99% and was supplied by Isotec Inc. The catalysts were first reduced in the reactor with 5% hydrogen in nitrogen stream (50 ml/min) at 700°C for 3 h prior to each catalytic measurement. Mixtures of CH_4/CO_2/He and CD_4/CO_2/He were alternatively introduced into the reactor after reaction for 2 h at each step, with a step interval of 50°C in the temperature range of 600 to 700°C. Space velocity of total gas mixture (GHSV) was 3×10^5 ml/h · g cat. The reactor effluent was analyzed with an on-line gas chromatograph (Chrompack Model CP 9001) with a capillary column (Chromapck carboPLOT P7) connected to a thermal conductivity detector. By performing the $CH_4 + CO_2$ and $CD_4 + CO_2$ reactions alternatively in this way, CH_4/CD_4 isotope effects could be investigated. The ratio in percentage of CO formed in the reaction to the total feed before reaction on the basis of carbon content was defined as the formation rate of CO. The relative ratios of CH_4 conversion in the $CH_4 + CO_2$ reaction to the corresponding ratios in the $CD_4 + CO_2$ reaction were used to express the magnitude of CH_4/CD_4 isotope effects.

Extended X-Ray Absorption Fine Structure (EXAFS) Analysis

X-ray absorption experiments were carried out mainly on beam line 10B at the Photon Factory of the National Laboratory for High Energy Physics (KEK-PF) in Tsukuba (Japan) with a ring energy of 2.5 GeV and stored current of 200–350 mA, and partially on beam line 3C at the Pohang Light Source (PLS) of Pohang Accelerator Laboratory (PAL) in Pohang (Korea) with the ring energy of 2.2 GeV and stored current of 150–250 mA. Details regarding the EXAFS measurements and data analysis were published elsewhere (33). X-ray absorption spectra were recorded in a transmission mode at room temperature with a Si(111) channel-cut monochromator. Higher harmonics in the beam were rejected by detuning the Si(111) monochromator crystals to give 80% of the maximum intensity. The transmission measurement geometry was arranged using gas-filled ionization chambers to monitor the intensities of the incident and transmitted X-rays. The gas ionization chambers were filled with an Ar/N_2 mixture to optimize sensitivity. The monochromator was scanned in energy with 0.5–2 eV steps starting from 250 eV below until 1000 eV above the Ni K-absorption edge ($E_0 = 8333$ eV). The energy steps in the absorption edge and extended X-ray absorption fine structure regions were 0.1 and 2 eV, respectively. For X-ray absorption measurement, about 0.1 g of the sample was pressed into thin wafers of 10 mm in diameter and treated in an *in situ* sample chamber prior to measurement at room temperature (33). The weight of samples was selected to achieve an absorption of less than $\mu x = 2.5$ for the calcined catalyst to optimize the signal to noise ratio and to avoid nonlinear variations of μx induced by the thickness of the sample pellet.

Analysis of the X-ray absorption data was carried out with a standard method using the UWXAFS2 program package (34) and FEFF 6.0 distributed by the University of Washington (35). To isolate the EXAFS from the X-ray absorption edge, a polynomial function characteristic of the background was subtracted. The EXAFS oscillations ($\chi(k)$) after background removal and normalization were k^3-weighted and Fourier-transformed within the limits $k = 2.0$–14.0 Å^{-1} to isolate the contributions of the different coordination shells. A curve-fitting procedure for FT data was employed to determine structural parameters, such as radial distance, R, and coordination number, N. The main peaks in the radial distribution function (RDF) were inverse-transformed into k space and least-squares calculations performed using the EXAFS equation $\chi(k)$ (35).

RESULTS

EXAFS Analysis

Figure 1 illustrates the Fourier transforms spectra of Ni K-edge EXAFS on Ni foil and NiO crystallite, and EXAFS data in k and r spaces of KNiCa/ZSI catalysts according to several treatments without the correction of the phase shift, where Fourier transformation was performed using the data in the range of $2.0 \leq k \leq 14.0$ Å^{-1}. The spectra of NiO and Ni foil as the references were obtained to decide the parameters for phase-shift (polynomial) and amplitude functions (Lorentzian). Those parameters were used to analyze the data of catalyst samples and to determine bond lengths (R) and coordination numbers (N) for Ni–Ni and Ni–O (34). To figure out the change of the local structure around the Ni atoms in the catalyst, we performed nonlinear curve-fitting analyses of the Fourier-filtered EXAFS of the first and second coordination shells of a nickel atom by a least-squares method. The fitting results are given in Table 1. In RDFs of a NiO reference, the peak appearing at 1–2 Å is due to the backscattering from the adjacent oxygen atoms, and the peak at 2–3 Å shows the presence of the second-neighboring nickel atoms (Fig. 1a). The peaks due to the backscattering from the nickel atoms are also seen in the high-distance region higher than 3 Å. Such a RDF pattern is characteristic of f.c.c. structure. On the KNiCa/ZSI catalyst after calcination, the magnitude of the peak appearing at 1–2 Å is almost constant, indicating that the number of oxygen atoms adjacent to Ni atoms is constant; i.e., Ni atoms in the catalyst keep their octahedral environment (Fig. 1c). This behavior is commonly observed from other groups' results on NiO–MgO catalysts (36) and Ni/SiO_2 catalysts (37). On the other hand, the magnitude of the peak appearing at 2–3 Å decreases remarkably and the peak pattern higher than 3 Å is considerably different from that of a NiO reference. This result implies that Si atoms of zeolite support would be partially occupied in the second coordination shells of a Ni atom (37). Although the second coordination shell is not exactly discerned into Ni–Ni and Ni–Si shells through curve-fitting analysis, the coordination number of the second shell is calculated as 9.8. When KNiCa/ZSI is reduced at 700°C for 1 h under 5% H_2 flow, a new peak at 1.5–2.5 Å appears (Fig. 1c). A new peak is ascribed to neighboring Ni atoms of first shell in metallic Ni environment. On the other hand, the magnitude of the peak appearing at 2–3 Å decreases and the amplitude of the peak at

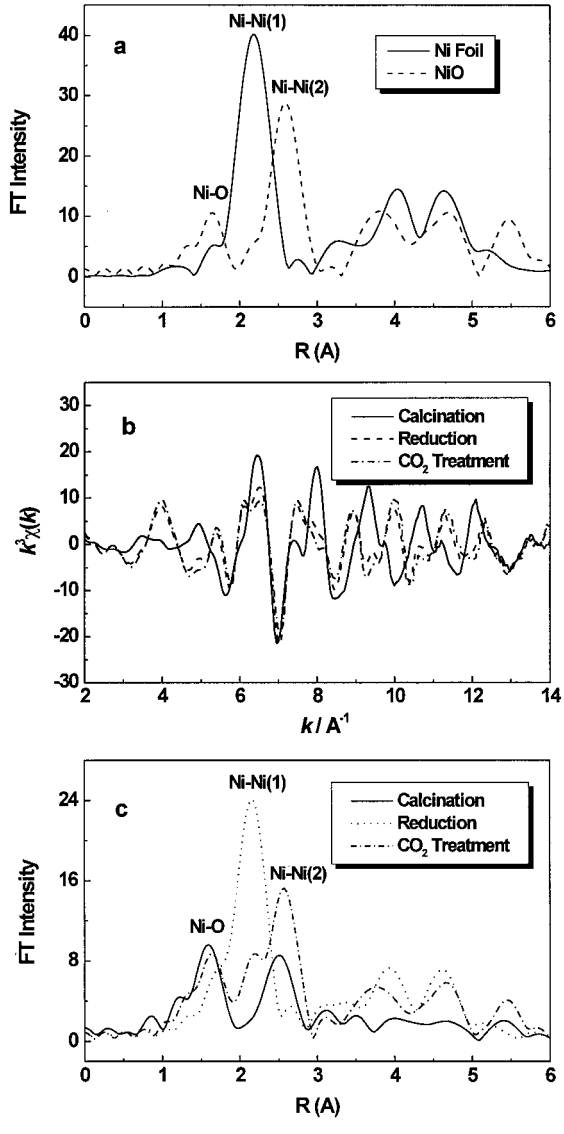

FIG. 1. Ni K-edge EXAFS for Ni foil, NiO, and KNiCa/ZSI catalysts. (a) Fourier transforms in r space of Ni foil (—) and NiO (-----); (b) k^3-weighted EXAFS oscillation, and (c) Fourier transforms in r space of KNiCa/ZSI catalysts after calcination in air at 650°C for 4 h (—), after reduction with 5% H_2 in N_2 at 700°C for 1 h (·····), and after treatment with 20% CO_2 in N_2 at 700°C for 30 min (– · –).

TABLE 1

Structural Parameters from EXAFS Ni K-Edge Analysis of KNiCa/ZSI Catalysts According to Pretreatment Conditions

Treatment condition	Atomic pair*	R/Å[a]	N[b]	$\Delta\sigma^2/10^{-4}$ Å[b,c]
Calcination in air at 650°C for 4 h	Ni–O	2.06	5.9	63
	Ni–Ni(O)	2.94	9.6	79
Reduction with 5% H_2 at 700°C for 1 h	Ni–O	2.09	3.2	79
	Ni–Ni(R)	2.47	9.1	78
	Ni–Ni(O)	2.96	1.1	81
Treatment with 20% CO_2 at 700°C for 0.5 h after reduction	Ni–O	2.04	6.9	78
	Ni–Ni(R)	2.46	2.3	79
	Ni–Ni(O)	2.94	11.7	84

[a] Nearest neighbor distance (±0.02).
[b] Nearest neighbor coordination number (±1.0).
[c] Difference in the Debye-Waller factor between samples and standards (±0.0005).
* Ni–Ni(R), Ni–Ni bond of metallic Ni; Ni–Ni(O), Ni–Ni bond of NiO. Reference: for NiO powder, Ni–O; $R = 2.09$ Å, $N = 6$; Ni–Ni(O); $R = 2.95$ Å, $N = 12$; For Ni foil, Ni–Ni(R); $R = 2.49$ Å, $N = 12$.

1–2 Å somewhat decreases together with a little change of peak position. It seems that there is only a trace of second-neighboring Ni atoms in the oxidized nickel domain due to its reduction while the nearest neighboring oxygen atoms in the oxidized nickel domain are partially lost. The number of nearest neighbors at the reduced nickel atoms is 9.1 for the reduced KNiCa/ZSI, which is lower than the value of 12 for metallic nickel.

It is considered that carbon dioxide is not an inert gas and, therefore, it can reoxidize a partly reduced surface (38). This oxidizing effect can be confirmed through EXAFS analysis. When the reduced KNiCa/ZSI catalyst is treated with 20% CO_2 at 700°C for 30 min, the amplitude of the metallic Ni–Ni bonds decreases (Fig. 1c and Table 1). After treatment with CO_2, peaks corresponding to Ni–O bond at 1–2 Å and Ni–Ni bond at 2–3 Å, respectively, reappear, indicating that the Ni clusters of the reduced catalyst are transformed into the oxidized Ni species by CO_2. On the other hand, the amplitude of the second coordination shell (Ni–Ni) peak is larger than that of the first coordination shell (Ni–O) peak, different from that of the calcined catalyst. This reflects the increase of coordination number in the second shell ($N = 11.7$) caused by increasing the crystallite size of oxidized Ni species. The number of first oxygen neighbors in the catalyst is calculated to be 6.9. In the case of nickel oxide with regular f.c.c. structure, the number of first oxygen neighbors to a central Ni atom should be limited to 6. However, it is probably assumed that Ni species are still surrounded by six oxygen atoms because the deviation from 6 coordination is within the error range of coordination number ($N \pm 1$). Consequently, these EXAFS results demonstrate that carbon dioxide can play a role as an oxidant on the nickel surface.

Catalytic Activity at Steady States

The KNiCa/ZSI catalyst exhibits high activity and high resistance against coke formation in the CO_2 reforming of methane, as shown in Fig. 2. Its high activity displayed in terms of CO_2 conversion attains to near equilibrium conversion (96.5%) of CO_2 to produce CO without catalyst deactivation at 800°C for 140 h. On the other hand, the Ni/ZSI catalyst is also highly active at initial period of reaction, but it is subjected to severe catalyst deactivation due to large coke deposition less than 40 h.

Pulse Reaction Analysis

The amounts of CO produced according to sequential injections of CO_2, CH_4 and CO_2 pulses at 600°C over the reduced KNiCa/ZSI catalyst are plotted in Fig. 3. It can be confirmed from these pulse reactions that the dissociative adsorption of CO_2 on the metallic Ni surface of KNiCa/ZSI catalyst produces CO and surface oxygen. The formation of CO is relatively large during the first several CO_2 pulses, but it decreases notably with increasing CO_2 pulse number. The

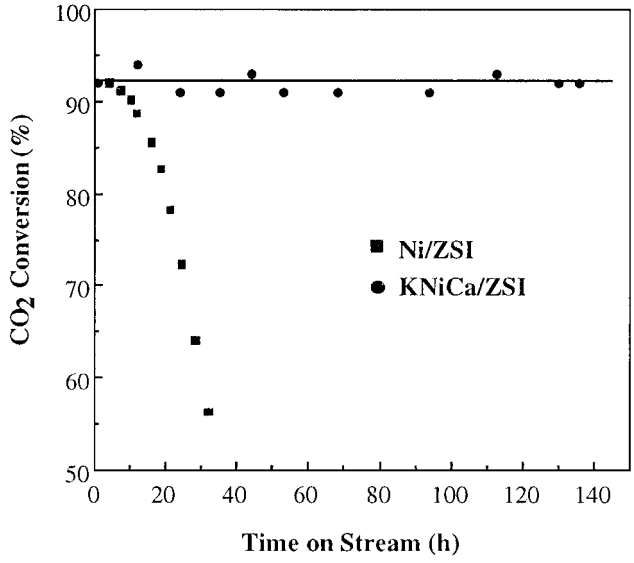

FIG. 2. Catalytic activity and stability of Ni/ZSI and KNiCa/ZSI catalysts for CO_2 reforming of methane in terms of CO_2 conversion. Reaction conditions: $T = 800$°C, $CH_4/CO_2/N_2 = 1:1:2.2$, GHSV $= 6.0 \times 10^4$ ml/h · g cat.

total amount of surface oxygen formed upon exposure to 10 pulses of CO_2 is estimated to 18.7 μmol, indicating that 21% of total Ni content on the catalyst would be oxidized. When the catalyst exposed to 10 pulses of CO_2 is subjected to CH_4 pulses, CO, CO_2, and H_2O are generated together with H_2. About 4.3 μmol of CO is formed during the first CH_4 pulse, and the amounts of CO formed during subsequent pulses are greatly diminished. This explains why oxygen species on the catalyst surface are formed together with the generation of CO during the injection of CO_2 pulses and remain on the catalyst surface even after stopping CO_2 pulses and flushing with inert gas. The amount of CO_2 and H_2O produced during these pulses are 3.3 and 6.5 μmol, respectively. The formation of H_2 (ca. 9.6 μmol) from 6 CH_4

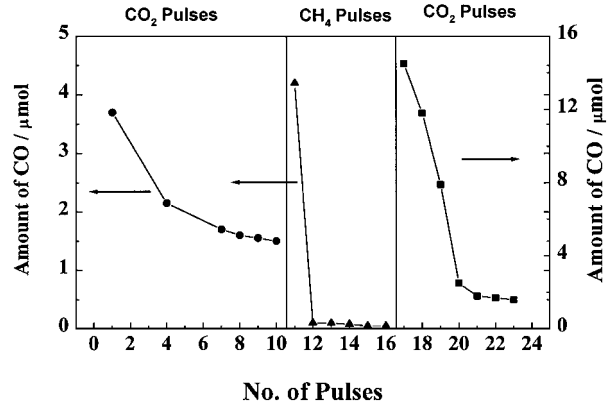

FIG. 3. Pulse test on the dissociation of CO_2 followed by the oxidation of CH_4 over the reduced KNiCa/ZSI catalyst at 600°C.

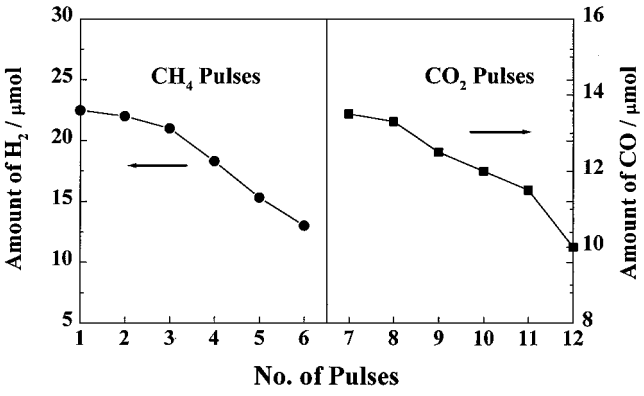

FIG. 4. Pulse test on the dissociation of CH_4 followed by CO_2 dissociation over the reduced KNiCa/ZSI catalyst via pulse reaction at 600°C.

pulses after the reaction with 10 CO_2 pulses is much lower than that on the freshly reduced catalyst, indicating the loss of hydrogen by its oxidation into water with the formed oxygen species from CO_2. When the catalyst is exposed again to a CO_2 pulse after sequential pulses of CO_2 and CH_4, the amount of CO produced increases four times higher than that of the reduced catalyst at initial stage.

Figure 4 provides the amount of H_2 or CO formed through sequential injections of CH_4 and CO_2 pulses at 600°C over the reduced KNiCa/ZSI catalyst. As compared to the integrated amount of CO produced during the same number of pulses, the activity of CH_4 dissociation is higher than that of CO_2 dissociation on the reduced catalyst. The amount of H_2 produced from CH_4 dissociation over this catalyst is gradually decreased with ordinal pulse number, which is different from the behavior of CO_2 dissociation during the injection of CO_2 pulses. When the catalyst is exposed to CH_4 pulses followed by CO_2 pulses, high activity for the CO formation is maintained even after the sixth CO_2 pulse. This indicates that surface carbon species are present on the catalyst after the CH_4 pulse and these species which are accumulated on the catalyst surface are originated mainly from the methane molecules rather than CO_2 molecules. As compared to the activity of the freshly reduced catalyst for the CO_2 pulse, higher catalytic activity on the CO_2 pulse after the CH_4 pulse seems to be ascribed mainly to the oxidation of surface carbon by CO_2 or surface oxygen. This step appears to be essential to the removal of surface carbon or the prevention of coke accumulation.

Gravimetric Analysis

Weight changes of supported Ni and KNiCa catalysts occurred during methane and subsequent CO_2 treatments are depicted in Fig. 5. It has been found that the maximum peak temperatures (T_{max}) for carbon deposition on these catalysts during the dry reforming are located at 570–630°C (31). For this reason, gravimetric analyses of the reduced catalysts toward methane decomposition were carried out at 600°C. When CH_4/He is flowed into the TGA reactor, the catalyst weight on Ni/ZSI is steeply increased with time, indicating the decomposition of methane to carbon and hydrogen. The amount of carbon deposited on the catalyst remains nearly constant after 1 h. Carbon deposition on KNiCa/ZSI is suppressed compared to that on Ni/ZSI, but it proceeds via two steps. These data obviously show that methane is more easily decomposed on the reduced surface of the Ni/ZSI catalyst than on the KNiCa/ZSI catalyst. It is further confirmed that decomposition activity of methane over Ni/ZSI (213 mg carbon/g cat) is eight times higher than that of KNiCa/ZSI (26 mg carbon/g cat), via weight gain on the catalysts during methane treatment. In addition, whisker-like carbon filaments have been observed over Ni/ZSI catalyst after the reaction (9); it is generally known that whisker-type carbon can be formed on supported Ni catalysts under methane decomposition (39). Ni dispersions of catalysts reduced at 700°C are 6.6% for Ni/ZSI and 2.0% for KNiCa/ZSI, respectively. Considering surface Ni dispersion and the increased weight after methane decomposition, the ratios of the formed carbon to surface Ni (C/Ni_s) on the catalysts are much higher than 1, indicating the formation of bulk-like carbon filaments together with surface carbon (31). After methane treatment these catalysts were flushed with helium gas and then treated with CO_2 up to 700°C. Changing the flowing gas to CO_2/He results in a fast decrease in the weight of the catalysts with increasing temperature from 430 to 470°C, because of the reaction of carbon with CO_2. After this

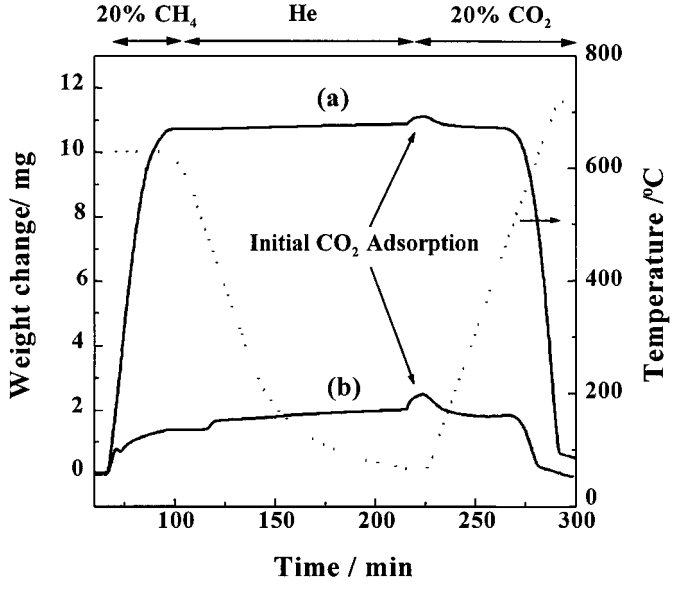

FIG. 5. Results on gravimetric analyses of zeolite-supported Ni catalysts depending on reactions with methane and carbon dioxide: (a) Ni/ZSI and (b) KNiCa/ZSI. Catalysts were carburized with 20% CH_4 diluted in He (50 ml/min) at 600°C for 30 min followed by oxidation with 20 vol% CO_2 diluted in He (50 ml/min) as increasing temperature in a rate of 10°C/min.

treatment the initial weight of KNiCa/ZSI catalyst is recovered, while the resulting weight of the Ni/ZSI catalyst is not fully recovered. A profile of its weight change by CO_2 treatment indicates that carbon species are still present on the Ni/ZSI catalyst. It is noted that even after treating the carburized Ni/ZSI catalyst with CO_2 up to 700°C, the weight of the used catalyst increased by 1.3 wt% compared to that of the fresh catalyst. Thus, carbon deposits on Ni/ZSI could not be completely gasified by CO_2 even at this temperature. These deposits could cause catalyst deactivation if they are continuously accumulated on catalysts under reaction conditions. This phenomenon was also reported by other researchers (40, 41). Shi *et al.* (40) found that carbon deposited from CH_4 for a longer period of time decreases the reactivity of the carbon toward CO_2 gasification, resulting in the buildup of carbon deposits on catalysts. Matsukata *et al.* (41) showed that the ungasified carbon was present in a moss-like morphology. The fact that the KNiCa/ZSI catalyst can be restored to its original weight indicates that carbon dioxide can oxidize deposited carbon, and therefore might be related to the removal of carbon on the catalyst.

The weight change of catalysts due to carbon formation during CO_2 reforming was also examined at 600°C. The amount of carbon deposits was estimated to be 4.9 mg carbon/g cat on KNiCa/ZSI for 1 h, and 54 mg carbon/g cat on Ni/ZSI under the same conditions (32). It is noted that all the carbon deposits on KNiCa/ZSI during the CO_2 reforming were formed within the initial 20 min of reaction, after which the accumulation of carbon ceased. This indicates that once the catalytic activity reaches steady state, carbon deposition via methane decomposition and carbon removal via CO_2 gasification are dynamically equilibrated with each other during the CO_2 reforming. Earlier work from our group also showed that methane decomposition is the major route responsible for carbon deposition, and that carbon dioxide in the reactant feed inhibits carbon deposition (30). The inhibiting effect of CO_2 on carbon deposition in a gas mixture of CO_2 and CH_4 can be ascribed to the CO_2 adsorption on active sites reacting with other surface species to produce CO.

Figure 6 shows differential profiles of weight loss of catalysts as a function of temperature during CO_2–TPO experiments, which were done after carburization of catalysts with methane at 600°C for 30 min. A CO_2–TPO peak maximum on the KNiCa/ZSI catalyst is centered at 590°C. For the Ni/ZSI catalyst, temperature maximum occurs at 690°C. A CO_2–TPO profile of Ni/ZSI suggests that CO_2 gasification of carbon on Ni/ZSI starts at 430°C which is earlier than that on KNiCa/ZSI, but it is not terminated at 700°C (see Fig. 5). In Fig. 6, the weight loss and mass number of a product generated from the carburized catalyst surface by CO_2 treatment with the increase of temperature are identified as CO. Moreover, it is noted that there is no formation of water on the carburized Ni surface during the CO_2–TPO experiment.

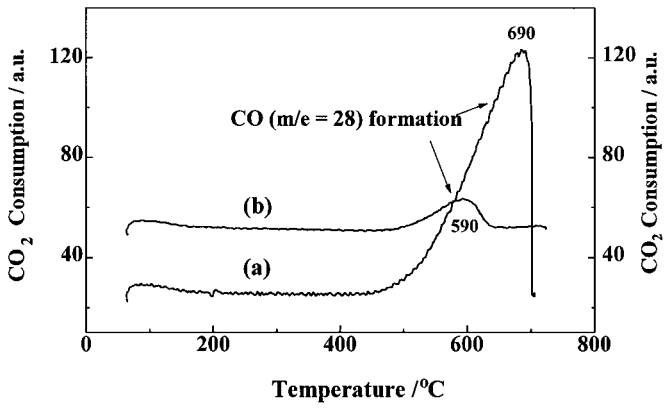

FIG. 6. CO_2–TPO profiles of supported Ni catalysts after carburization with 20 vol% CH_4 diluted in He (50 ml/min) at 600°C for 1 h: (a) Ni/ZSI and (b) KNiCa/ZSI. In CO_2–TPO runs, carburized catalysts were oxidized with 20 vol% CO_2 diluted in He (50 ml/min) as increasing temperature in a rate of 10°C/min.

Hence, it is assumed that surface carbon species formed on the catalyst are present mainly as a type of Ni–C(s).

On the other hand, the reactivity of the KNiCa/ZSI catalyst for the CO_2 dissociation at 600°C is larger than that of Ni/ZSI at the same temperature (32). From gravimetric analyses of the catalysts during the treatment with diluted CO_2 (20%) for 1 h, it is observed that the weight gain due to the formation of surface oxygen from the dissociation of carbon dioxide is much higher on KNiCa/ZSI (7.5 mg oxygen/g cat) than Ni/ZSI (1.1 mg oxygen/g cat).

Deuterium Isotope Effect

The results of the deuterium isotope experiment for the dry reforming to synthesis gas over the Ni/ZSI and KNiCa/ZSI catalysts are summarized in Table 2. Before

TABLE 2

The Relationships of the Activities in the CO_2 Reforming of Methane over ZSI-Supported Ni Catalysts by using CH_4/CO_2 and CD_4/CO_2 Gas Mixtures

Catalyst	Temperature (°C)	$R_{CH_4}(CH_4)^a$ (μmol/s · g cat)	$R_{CD_4}(CD_4)^b$ (μmol/s · g cat)	$R_{CH_4}/R_{CD_4}{}^c$
Ni/ZSI	600	57.5	49.6	1.16
	650	139	128	1.09
	700	425	409	1.04
KNiCa/ZSI	600	54.9	52.3	1.05
	650	134	130	1.03
	700	443	441	1.00

[a] $R_{CH_4}(CH_4)$: the absolute rate of CH_4 consumption for CH_4/CO_2 mixture.

[b] $R_{CD_4}(CD_4)$: the absolute rate of CD_4 consumption for CD_4/CO_2 mixture.

[c] R_{CH_4}/R_{CD_4} corresponds to the relative ratio on the rates of CH_4 consumption obtained when using a CH_4/CO_2 mixture to that when using a CD_4/CO_2 mixture.

switching the mixture from $CH_4/CO_2/He$ to $CD_4/CO_2/He$, the reaction at each temperature was run to reach stable performance of the catalysts for at least 1 h. Although the rate of CH_4 consumption, R_{CH_4}, is slightly affected by replacement of CH_4 with CD_4 at 600°C, this rate over the KNiCa/ZSI catalyst is almost unchanged upon replacing CH_4 with CD_4 in feed mixtures at 700°C, indicating that the dissociation of the C–H bond of CH_4 molecule is a fast step over the KNiCa/ZSI catalyst. However, a small but discernible reduction in the rate of CH_4 consumption over the Ni/ZSI catalyst is observed when CH_4 is replaced with CD_4, i.e., the value of the R_{CH_4}/R_{CD_4} ratio amounts to 1.16–1.04 at 600–700°C. The mild isotope effect on Ni/ZSI may be due to the surface structure of the Ni crystals as illustrated in a comprehensive review of Bradford and Vannice (28). This ratio is also temperature dependent, increasing with decreasing the reaction temperature. This indicates that the catalytic activity is significantly affected by the replacement of CH_4 with CD_4 at lower temperature, i.e., activity decrease, since carbon monoxide can also be formed via the RWGS reaction ($CO_2 + H_2 \rightarrow CO + H_2O$) which is thermodynamically favorable at lower temperatures. On the other hand, a very weak deuterium isotope effect over KNiCa/ZSI indicates that the rate of CH_4 dissociation is not affected by the rate of RWGS reaction, implying that the adsorbed carbon species is not expected to contain any hydrogen atom(s). This phenomenon corresponds to Zhang and Verykios' observation over Ni/γ–Al_2O_3 catalysts (20). As a result, the CH_4 dissociation is excluded from the rate-determining step since this seems to proceed rapidly as described above. Instead, the surface reaction of adsorbed carbon species and adsorbed oxygen or surface carbonate species is probably rate determining step for the dry reforming.

DISCUSSION

The Role of Support and Alkaline Promoters

It has been generally observed that the nature of the support greatly affects catalytic performance in dry reforming (2, 5, 8, 9). The selection of a suitable support is regarded as one of the key aspects for designing a stable catalyst for the reaction (42). Indeed some supported nickel catalysts have shown promising activity and long life without obvious deactivation through the selection of a suitable support (2, 5, 8, 9). Zhang *et al.* (8) attributed the remarkable stability of Ni/La_2O_3 compared to Ni/γ–Al_2O_3 or Ni/CaO to the interaction of carbon dioxide with the La_2O_3 support to form lanthanum carbonate, which scavenges carbon from nickel at the Ni–La_2O_3 interface, thus restoring the Ni particles to their original state (21). Fujimoto and co-workers (5) reported that an excellent catalyst is a MgO support for forming a nickel magnesia solid solution catalyst, $Ni_{0.03}Mg_{0.97}O$. It has been also shown that a ZrO_2 support for Pt catalysts is very effective toward the dry reforming (2, 42, 43). In that case, the catalytic activity of Pt/ZrO_2 catalysts was explained in terms of the CO_2 activation via carbonate species on the support which must be in the proximity of the Pt particles to react with the methane activated on the metal (42, 43). We also found that the composite support which is composed of a highly siliceous NaZSM-5 zeolite and an alumina binder offers high catalyst stability for the KNiCa catalyst compared with a highly siliceous NaZSM-5 zeolite itself, γ-Al_2O_3 and SiO_2 supports (32). Thus, it is most likely that besides the role of alkaline promoters, high catalyst stability for KNiCa/ZSI is partially originated from a synergistic effect due to the contribution of each component.

It is assumed that a zeolite component in ZSI-supported Ni catalysts plays a role in minimizing the formation of $NiAl_2O_4$ spinel due to the presence of microporous zeolite, which is considered to be a factor of catalyst aging (39). Besides, it is pointed out as another characteristic that ZSM-5-type zeolite is the most thermally stable among many zeolite molecular sieves, and a favorable adsorbent for carbon dioxide. Although it is rare, some reports have dealt with the utilization of zeolite as a support for Ni catalyst in the dry reforming (44–46). Li *et al.* also used ZSM-5 zeolite support for dry reforming in order to utilize its good physical and chemical properties (45). On the other hand, the role of the alumina component in the KNiCa/ZSI catalyst was considered to form a $CaAl_2O_4$ phase through solid-state reaction with calcium oxide which suppresses the coke formation as well as the formation of $NiAl_2O_4$ spinel (30, 32). This phase was identified by XRD and solid-state ^{27}Al NMR analyses. It is noted that the $CaAl_2O_4$ phase formed in the catalyst is known as a good support for steam-reforming catalysts (4, 39).

The metallic Ni and CaO or K_2O sites adjacent to reduced nickel metal sites on the KNiCa/ZSI catalyst are regarded as sites for CO_2 chemisorption. The chemisorbed amount of CO_2 on the KNiCa/ZSI catalyst is 40% higher than that of the Ni/ZSI catalyst (32). As shown in the CO_2 desorption profiles of Fig. 7, the integrated amount of CO_2 desorption on the KNiCa/ZSI catalyst is higher than that on the Ni/ZSI catalyst, which corresponds with the results of volumetric CO_2 adsorption. In addition, a significant difference in the CO_2–TPD profiles for Ni/ZSI and KNiCa/ZSI catalysts is observed in the high temperature region. A CO_2–TPD profile of KNiCa/ZSI exhibits a strong desorption peak above 600°C, which is not observed on Ni/ZSI. The desorption peak at higher temperatures indicates the formation of surface carbonate, mainly on a Ca promoter due to its high composition and, therefore, the presence of this peak seems to be directly related to the excellent stability of KNiCa/ZSI compared to Ni/ZSI.

Previous FT-IR observations of the reduced catalysts revealed that the behavior of adsorbed CO_2 on KNiCa/ZSI is

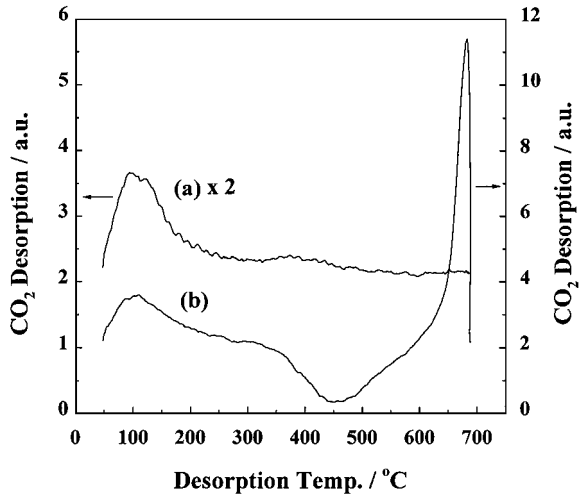

FIG. 7. CO_2–TPD profiles of reduced (a) Ni/ZSI and (b) KNiCa/ZSI catalysts ($\beta = 10^{\circ}$C/min).

greatly different from that on Ni/ZSI (47). The IR spectrum of the reduced KNiCa/ZSI catalyst upon the CO_2 adsorption or the reforming reaction showed two distinct bands at 1480 and 1410 cm^{-1}, which are assigned to asymmetric (ν_{as}(OCO)) and symmetric stretching vibration (ν_s(OCO)) modes of monodentate carbonate species (47), respectively. These species were supposed to be coordinated to calcium or potassium oxide of the catalyst. However, these bands were not present on the Ni/ZSI catalyst. The formation of carbonate species on the CO_2 adsorption sites of the basic catalyst surface would be closely related to the high stability of the KNiCa/ZSI catalyst due to the inhibition of coke deposition on its nickel surface. Thus the enrichment of surface carbonate species upon CO_2 adsorption may take part in the elimination of coke by converting it into CO. Indeed the importance of carbonate for the dry reforming has been previously pointed out by several authors (21, 43).

The presence of alkali and alkaline earth metals could offer several effects for the physicochemical properties of the reforming Ni catalyst (48–50), i.e., (a) electronic properties of the Ni clusters as well as their dimensions, (b) the modification of surface acidity of support, and (c) surface enrichment of CO_2 through the stabilization of surface carbonate species. Alkaline metal atoms such as K and Ca can modify the local electron density and particle size of metallic Ni clusters. The change of reducibility of nickel would be responsible for the modification of its electronic property. The addition of potassium resulted in either a promoting or poisoning effect. It has been shown that the addition of 0.6 wt% K on Ni/ZSI catalyst improves catalyst stability without loss of catalytic activity, while with an increase of the potassium content above 1 wt%, the promotion effect on catalyst stability is suppressed by some poisoning function of potassium due to the surface coverage to active sites, resulting in remarkable loss of catalytic activity. Therefore, the composition of potassium on KNiCa/ZSI catalyst is desirable at less than 1 wt%. In contrast to the case of potassium, the catalytic activity was not affected much by the content of calcium in the catalyst. In addition to these, many studies suggest that alkaline metal oxides can neutralize the surface acidic sites of reforming catalysts, thus enhancing their resistance to poisoning via acid-catalyzed carbonaceous species from polymerization of the CH_x or C_x groups (51). Although promotional effects upon the addition of alkaline metals can not be separated distinctly according to each factor, the most important role of alkaline promoters in the catalyst is considered to be surface enrichment of CO_2 as a kind of CO_2 pool through the stabilization of surface carbonate species and their participation in the removal of carbonaceous species.

The ungasified carbon on Ni/ZSI would be the origin of catalyst deactivation if it is accumulated on the catalyst without complete removal under given reaction condition as shown in Fig. 7. Therefore, it is possible that CO_2 gasification of carbon on KNiCa/ZSI is cooperatively promoted by the addition of K and Ca promoters. This can be further supported by the following bases. It is known that alkali and alkaline earth oxides and salts including K and Ca are the best catalysts for the gasification reactions of carbon by CO_2 as well as H_2O, which are the bases of coal gasification processes (52, 53). For example, many types of active intermediates such as $CaCO_3$, CaO, CaO_2, and Ca_xO_y have been proposed for calcium-catalyzed gasification reactions (53). Heinemann and Somorjai (54) also reported that KNiCa oxide catalysts are very highly selective on C_{2+} hydrocarbons in the oxidative coupling of methane (OCM) via cofeeding with steam. Their OCM activities partially originated from the activity for steam gasification of carbon. Besides, Haga *et al.* (55) found that the role of Ca added in Ni-catalyzed hydrogasification of carbon is to supply *in situ* active oxygen to the Ni–C interface during the reaction to promote the nickel catalysts and prevent the coke formation. Therefore, it is supposed that carbon dioxide forms a surface $CaCO_3$ species with surface CaO on the catalyst, leading to partial conversion of surface carbon on nickel into CO via oxygen transfer under reaction conditions.

Mechanistic Consideration

In connection with the results described above, we propose the elementary reaction steps plausible to describe the mechanism for the dry reforming over the KNiCa catalyst in the following way. The first step of methane activation consists of reversible reaction between methane molecules and surface Ni sites, leading to adsorbed carbon species and gaseous hydrogen (step [1]) through stepwise dissociation of methane. What happens to the adsorbed hydrogen species cannot be ascertained from the present

experiments, but it may be assumed that these species desorb mainly as H_2 because of no evidence of surface hydrogen accumulation. Surface carbon species formed on the catalyst are present probably as a type of Ni–C(s) or carbide-like species which contains no C–H bond.

$$CH_4(g) + Ni(s) \rightleftarrows Ni\text{–}C(s) + 2H_2(g), \quad [1]$$

where s is surface adsorbed species and g is gas phase species.

The dissociative adsorption of carbon dioxide occurred mainly on different Ni sites, leading to surface oxygen and gaseous CO according to step [2]. This step is slower than the methane dissociation but not rate determining. Carbon monoxide formed in step [2] would be immediately released into the gas phase, as observed by the earlier IR study of our group (30) and studies of CO_2 activation on metallic nickel reviewed by Solymosi (56),

$$CO_2(g) + Ni(s) \rightleftarrows Ni\text{–}O(s) + CO(g). \quad [2]$$

Then, the Ni surface of the catalyst is mostly occupied by adsorbed carbon and oxygen species as reaction intermediates during the reaction. The surface reaction of these species produces gaseous CO and simultaneously rejuvenated nickel species (step [3]), which is assumed to be the rate-determining step under our reaction condition. This assumption can be supported by the fact that this step requires surface migration of surface species (17),

$$Ni\text{–}C(s) + Ni\text{–}O(s) \rightarrow CO(g) + 2Ni(s). \quad [3]$$

The surface reaction of these species seems to be proceeded by the Langmuir-Hinshelwood mechanism. This is similar to the pyrolysis mechanism in which CO is generated by the oxidation of surface carbon species formed via the CH_4 dissociation (57). If this step is not facilitated during the reaction, carbon deposition would be predominant and as a consequence catalyst would be deactivated by severe coke accumulation.

Carbon dioxide either directly in the gas phase or as surface carbonates can also react with surface carbon species arising from methane dissociation according to step [4] or [5], assuming that these reactions reach equilibrium overall (17). It seems that step [4] or [5] is essential for maintaining highly stable activity by the removal of surface carbon species. As a result, over KNiCa/ZSI catalysts the accumulation of surface carbon species is suppressed by the function of surface carbonates or CO_2 gasification of carbon which is facilitated by the presence of alkaline promoters,

$$CO_2(g) + Ni\text{–}C(s) \rightarrow 2CO(g) + Ni(s) \quad [4]$$

or

$$CO_2(s) \text{ as carbonates} + Ni\text{–}C(s) \rightarrow 2CO(g) + Ni(s). \quad [5]$$

Although it is not quantitatively discussed in this work, the formation of water should also be taken into account because the water is inevitably formed during the dry reforming reaction. Besides in steps [2] and [4], carbon dioxide can also be dissociated by hydrogen species on Ni sites to yield surface hydroxyl and gaseous CO according to step [6], as similar to the suggestion of Bradford and Vannice (22). These steps would be further followed by step [7] to yield water,

$$CO_2(g) + Ni\text{–}H(s) \rightleftarrows Ni\text{–}OH(s) + CO(g) \quad [6]$$

$$Ni\text{–}OH(s) + Ni\text{–}H(s) \rightleftarrows 2Ni + H_2O(s) \rightleftarrows H_2O(g). \quad [7]$$

The plausible combination of hydrogen adsorption and these two steps represents the RWGS equilibrium. In the present work the contribution of step [6] to the formation of CO may not be so significant and this step may be temperature dependent because the rates of CO production on the supported Ni catalysts were only slightly affected by replacement of CH_4 with CD_4 as well as the concentration of water produced during the reaction which was much lower than that of CO. As previously shown (30), the H_2/CO ratio in the product stream over ZSI-supported Ni catalysts was less than one as expected from the stoichiometric reforming reaction, which is affiliated with the RWGS reaction. This reaction consumes part of H_2 produced from methane decomposition through the reaction of H_2 with CO_2 to yield CO and water. At higher temperatures ($>700^\circ$C) the H_2/CO ratio is close to one because the dry reforming becomes gradually predominant and the water formed from RWGS can be consumed by the steam-reforming reaction to produce H_2 and CO.

CONCLUSIONS

It is clearly shown that metallic Ni sites have strong reactivity with methane, while alkaline promoters do with carbon dioxide. Zeolite-supported Ni catalysts without alkaline promoters are readily deactivated due to the high reactivity toward methane to cause severe carbon deposition on the surface. In contrast, zeolite-supported KNiCa catalyst has very stable activity due to the retardation effect of alkaline promoters to coke deposition, which is attributed to surface enrichment of carbon dioxide by way of carbonate species. Because coke deposition is mainly caused by methane decomposition, the catalyst surface covered with adsorbed CO_2 as carbonate species or reactive oxygen species from the dissociation of CO_2 would prevent coke deposition. The addition of alkaline promoters also seems to greatly suppress the activity of supported Ni catalyst for the direct decomposition of methane. It is also found that the dissociation of CO_2 and CH_4 in the CO_2 reforming of methane are initial steps in the production of CO and H_2, respectively. However, the surface reaction of adsorbed

carbon (Ni–C(s)) and oxygen (Ni–O(s)) species to produce carbon monoxide is proposed as a rate-determining step in this reaction. This step obviously leads to the regeneration of metallic nickel species to be necessary for maintaining high catalyst stability during the reaction. In addition, the oxidation step of surface carbon with gaseous CO_2 or surface carbonates over KNiCa/ZSI catalyst is also considered to eliminate surface carbon species effectively.

ACKNOWLEDGMENTS

Financial support by the Ministry of Environment (MOE) and the Ministry of Science and Technology (MOST) in Korea is gratefully acknowledged. The authors are indebted to Professor R. Ryoo and Dr. C. Pak, Department of Chemistry, Korea Advanced Institute of Science Technology (KAIST), for their support with the EXAFS analyses. We also thank Mr. M. S. Park, H. S. Roh, and Ms. E. K. Lee for technical assistance in the experimental work. Dr. C. W. Lee, Dr. Y. K. Park, and Dr. W. Y. Kim are gratefully acknowledged for helpful discussions. The EXAFS experiment was partially supported by the Photon Laboratory in Japan. The X-ray absorption experiments at the Ni K edge were also performed under the approval of the Photon Factory Program Advisory Committee. Experiments at PLS were supported in part by MOST and POSCO.

REFERENCES

1. Ashcroft, A. T., Cheetham, A. K., Green, M. L., and Vernon, P. D. F., *Science* **352**, 225 (1991).
2. van Keulen, A. H. J., Seshan, K., Hoebink, J. H. B. J., and Ross, J. R. H., *J. Catal.* **166**, 306 (1997).
3. Rostrup-Nielsen, J. R., *Stud. Surf. Sci. Catal.* **81**, 25 (1993).
4. Gadalla, A. M., and Bower, B., *Chem. Eng. Sci.* **43**, 3049 (1988).
5. Yamazaki, O., Nozaki, T., Omata, K., and Fujimoto, K., *Chem. Lett.* 1953 (1992).
6. Slagtern, A., Olsbye, U., Blom, R., Dahl, I. M., and Fjellvag, H., *Appl. Catal.* **145**, 375 (1996).
7. Kroll, V. C. H., Swaan, H. M., and Mirodatos, C., *J. Catal.* **161**, 409 (1996).
8. Zhang, Z., Verykios, X. E., MacDonald, S. M., and Affrossman, S., *J. Phys. Chem.* **100**, 744 (1996).
9. Chang, J.-S., Park, S.-E., Lee, K. W., and Choi, M. J., *Stud. Surf. Sci. Catal.* **84**, 1587 (1994).
10. Li, X., Chang, J.-S., and Park, S.-E., *Chem. Lett.*, 1099 (1999).
11. Richardson, J. T., and Paripatyadar, S. A., *Appl. Catal.* **61**, 293 / (1990).
12. Solymosi, F., Kutsan, G., and Erdohelyi, A., *Catal. Lett.* **11**, 149 (1991).
13. Bitter, J. H., Halley, W., Seshan, K., Niessan, W., and Lercher, J. A., *Catal. Today* **29**, 349 (1996).
14. Seshan, K., ten Barge, H. W., Halley, W., van Keulen, A. N. J., and Ross, J. R. H., *Stud. Surf. Sci. Catal.* **81**, 285 (1994).
15. Rostrup-Nielsen, J. R., and Bak Hansen, J.-H., *J. Catal.* **144**, 38 (1993).
16. Wang, H.-Y., and Au, C.-T., *Catal. Lett.* **38**, 77 (1996).
17. Kroll, V. C. H., Swaan, H. M., Lacombe, S., and Mirodatos, C., *J. Catal.* **164**, 387 (1997).
18. Turlier, P., Pereira, E. B., and Martin, G. A., Proc. Int. Conf. on CO_2 Utilization, Bari, p. 119, 1993.
19. Gamman, J. J., Millar, G. J., Rose, G., and Drennan, J., *J. Chem. Soc., Faraday Trans.* **94**, 701 (1998).
20. Zhang, Z. L., and Verykios, X. E., *Catal. Lett.* **38**, 175 (1996).
21. Slagtern, A., Schuurman, Y., Leclercq, C., Verykios, X., and Mirodatos, C., *J. Catal.* **172**, 118 (1997).
22. Bradford, M. C. J., and Vannice, M. A., *Appl. Catal. A* **142**, 97 (1996).
23. Aparicio, L. M., *J. Catal.* **165**, 262 (1997).
24. Osaki, T., Horiuchi, T., Suzuki, K., and Mori, T., *Catal. Lett.* **44**, 19 (1997).
25. Osaki, T., Fukaya, H., Horiuchi, T., Suzuki, K., and Mori, T., *J. Catal.* **180**, 106 (1998).
26. Hu, Y. H., and Ruckenstein, E., *J. Phys. Chem. B* **101**, 7563 (1997).
27. Wolf, D., Barre-Chassonnery, M., Hohenberger, M., van Veen, A., Baerns, M., *Catal. Today* **40**, 147 (1998).
28. Bradford, M. C. J., and Vannice, M. A., *Catal. Rev.-Sci. Eng.* **41**(1), 1 (1999).
29. Au, C.-T., Ng, C.-F., and Liao, M.-S., *J. Catal.* **185**, 12 (1999).
30. Chang, J.-S., Park, S.-E., and Chon, H., *Appl. Catal.* **144**, 111 (1996).
31. Chang, J.-S., Park, S.-E., Roh, H. S., and Park, Y. K., *Bull. Kor. Chem. Soc.* **19**, 809 (1998).
32. Chang, J.-S., Ph.D. dissertation, KAIST, Korea (1996).
33. Cho, I. H., Park, S. B., Cho, S. J., and Ryoo, R., *J. Catal.* **173**, 295 (1998).
34. Frenkel, A. I., Stern, E. A., Qian, M., and Newville, M., *Phys. Rev. B* **48**, 12449 (1993).
35. Newville, M., Livins, P., Yacoby, Y., Rehr, J. J., and Stern, E. A., *Phys. Rev. B* **47**, 14126 (1993); Stern, E. A., *Phys. Rev. B* **48**, 9825 (1993).
36. Yoshida, T., Tanaka, T., Yoshida, H., Funabiki, T., and Yoshida, S., *J. Phys. Chem.* **100**, 2302 (1996).
37. Clause, O., Kermarec, M., Bonneviot, L., Villain, F., and Che, M., *J. Am. Chem. Soc.* **114**, 4709 (1992).
38. Krylov, O. V., and Mamedov, A. K., *Ind. Eng. Chem. Res.* **34**, 474 (1995).
39. Rostrup-Nielsen, J. R., *in* (J. R. Anderson and M. Boudart, Eds.), "Catalysis Science and Technology" Vol. 5, p. 1. Springer-Velag, Berlin, 1984.
40. Shi, J., Zhang, J., and Zhang, L., *Nat. Gas. Chem. Eng.* **20**, 14 (1995).
41. Matsukata, M., Matsushita, T., and Ueyama, K., *Chem. Eng. Sci.* **51**, 2769 (1996).
42. Bitter, J. H., Seshan, K., and Lercher, J. A., *J. Catal.* **171**, 279 (1997).
43. Bitter, J. H., Seshan, K., and Lercher, J. A., *J. Catal.* **176**, 93 (1998).
44. Kim, G. J., Cho, D. S., and Kim, K. H., *Catal. Lett.* **28**, 41 (1994).
45. Li, W. Y., Feng, J., and Xie, K. C., *Petrol. Sci. Tech.* **16**, 539 (1998).
46. Song, C., Murata, S., Srinvas, S. T., Sun, S., and Scaroni, A. W., *Prepr. Am. Chem. Soc. Div. Petroleum Chem.* **44**, 160 (1999).
47. Park, S.-E., Chang, J.-S., Roh, H. S., Anpo, M., and Yamashita, H., *Stud. Surf. Sci. Catal.* **114**, 395 (1998).
48. Diaz, A., Acosta, D. R., Odriozola, J. A., and Moutes, M., *J. Phys. Chem. B* **101**, 1782 (1997).
49. Huang, C. D., Richardson, J. T., *J. Catal.* **51**, 1 (1978).
50. Goodman, D. W., and Kiskinova, M., *Surf. Sci.* **105**, L265 (1981).
51. Mross, W. D., *Catal. Rev. Sci. Eng.* **25**, 591 (1983).
52. Chen, S. G., and Yang, R. T., *Energy Fuels* **11**, 421 (1997).
53. Lizzio, A. A., and Radvic, L. R., *Ind. Eng. Chem. Res.* **30**, 1735 (1991).
54. Rasko, J., Somorjai, J. A., and Heinemann, H., *Appl. Catal. A* **84**, 57 (1992).
55. Haga, T., Ozaki, J.-I., Suzuki, K., and Nishiyama, Y., *J. Catal.* **134**, 107 (1992).
56. Solymosi, F., *J. Mol. Catal.* **65**, 337 (1991).
57. Hu, Y. H., and Ruckenstein, E., *Catal. Lett.* **34**, 41 (1995).